

## Article

# Robotic Disassembly of Electric Vehicles' Battery Modules for Recycling

Ian Kay, Siamak Farhad <sup>\*</sup>, Ajay Mahajan <sup>\*</sup>, Roja Esmaeeli and Sayed Reza Hashemi

Department of Mechanical Engineering, College of Engineering and Polymer Science, The University of Akron, Akron, OH 44325, USA; ipk2@uakron.edu (I.K.); re25@uakron.edu (R.E.); sh184@uakron.edu (S.R.H.)

<sup>\*</sup> Correspondence: sfarhad@uakron.edu (S.F.); majay@uakron.edu (A.M.)

**Abstract:** Manual disassembly of the lithium-ion battery (LIB) modules of electric vehicles (EVs) for recycling is time-consuming, expensive, and dangerous for technicians or workers. Dangers associated with high voltage and thermal runaway make a robotic system suitable for the automated or semi-automated disassembly of EV batteries. In this paper, we explore battery disassembly using industrial robots. To understand the disassembly process, human workers were monitored, and the operations were analyzed and broken down into gripping and cutting operations. These operations were selected for automation, and path planning was performed offline. For the gripper, a linear quadratic regulator (LQR) control system was implemented. A system identification method was also implemented in the form of a batch least squares estimator to form the state space representation of the planar linkages used in the control strategy of the gripper. A high-speed rotary cut-off wheel was adapted for the robot to perform precise cutting at various points in the battery module case. The simulation results were used to program an industrial robot for experimental validation. The precision of the rotary cutter allowed for a more direct disassembly method as opposed to the standard manual method. It was shown that the robot was almost twice as fast in cutting but slower in pick and place operations. It has been shown that the best option for disassembly of a LIB pack is a human-robot collaboration, where the robot could make efficient cuts on the battery pack and the technician could quickly sort the battery components and remove connectors or fasteners with which the robot would struggle. This collaboration also reduces the danger encountered by the technician because the risk of shorting battery cells while cutting would be eliminated, but the time efficiency would be significantly improved. This paper demonstrates that a robot offers both safety and time improvements to the current manual disassembly process for EV LIBs.

**Keywords:** lithium-ion battery; recycling; robots; automation; electric/hybrid vehicles



**Citation:** Kay, I.; Farhad, S.; Mahajan, A.; Esmaeeli, R.; Hashemi, S.R. Robotic Disassembly of Electric Vehicles' Battery Modules for Recycling. *Energies* **2022**, *15*, 4856. <https://doi.org/10.3390/en15134856>

Academic Editor: Cai Shen

Received: 9 June 2022

Accepted: 29 June 2022

Published: 2 July 2022

**Publisher's Note:** MDPI stays neutral with regard to jurisdictional claims in published maps and institutional affiliations.



**Copyright:** © 2022 by the authors. Licensee MDPI, Basel, Switzerland. This article is an open access article distributed under the terms and conditions of the Creative Commons Attribution (CC BY) license (<https://creativecommons.org/licenses/by/4.0/>).

## 1. Introduction

Robotic systems have been widespread in usage for the assembly of lithium-ion batteries (LIBs) for many years, but their use for disassembly has only recently been considered as hybrid electric vehicles (HEVs) and electric vehicles (EVs) become more prevalent. As the adoption of EVs and HEVs gains traction, the value of the active materials, such as lithium cobalt oxide (LiCoO<sub>2</sub>) and lithium nickel manganese cobalt oxide (LiNiMnCoO<sub>2</sub>), within the batteries is lost if they are not recycled [1–3]. To prepare for the end of life (EOL) of these battery systems, the recycling process for LIBs is being researched to reduce not only the environmental impact of landfilling LIBs but also to recover the valuable materials contained within the LIBs [4–6]. It has been shown that the robotic disassembly of an HEV battery system is possible [7], but more work is required in this field for proof of concept.

Most LIB recycling is done through pyrometallurgical [8], hydrometallurgical [9,10], and physical/direct processes [11]. These methods may rely on the disassembly and shredding of battery cells/modules/packs before the process begins to reduce the contaminants created by the case and structural materials used in the construction of modules and

packs. The disassembly process allows for the sorting of bulk materials, such as aluminum, structural plastics, printed circuit boards (PCBs) and integrated circuits (ICs), copper, and various other components [9]. In the physical/direct recycling process, once these materials are removed, either individual cells or modules can be put into a shredder to separate the materials contained within the cells. The shredded cells or modules then undergo a physical separation process and are submerged in an alkali solution of lithium brine. This process allows the various materials to be sorted via physical and chemical means, increasing the purity of the filter/powder cake [12] and making the various by-products suitable for secondary processing.

Currently, more than 95% of LIBs are landfilled each year [13]. In addition, the total number of unrecycled batteries are increasing because of their adoption in EV applications [13]. Some of the major challenges in LIB recycling are due to the economics of the recycling process. Currently, the costs associated with the recycling of LIBs may be enough to make recycling unsustainable without subsidies or mandates due to the recovered value of materials being less than the required resources. One cost that significantly impacts the recycling process is the labor associated with the disassembly of packs and modules. This step in the recycling process is both time consuming and hazardous to the technicians/laborers. The manual disassembly process requires a technician/laborer to operate hand tools to remove fasteners, connectors, wires, and cut tabs, which can be difficult due to the pack layout and location of various hardware components within the pack assembly. In addition, the technician/laborer must wear personal protection equipment (PPE) and handle the tools with extreme care, as any mistake in the disassembly process could present hazards to the technician/laborer in the form of electrocution or explosion. Hazards associated with the disassembly process are a result of the high voltage in the battery system if it is not properly discharged and thermal instability if the individual cells are mechanically, electrically, or thermally compromised. The hazards can be mitigated through the proper pre-disassembly procedures, but caution should always be taken when handling the packs for disassembly.

To reduce the economic burden associated with the disassembly process, a robotic method for automating or semi-automating the disassembly process was envisioned and tested in disassembling a representative battery module. This process was broken down into the following steps: process identification, suitable actions for robotic implementation, end-of-arm tooling design and control, development of a representative work piece, workspace layout, path planning, robotic modelling and simulation in MATLAB/Simulink, and experimental testing of the robotic system. The research focused on the implementation of a robot for disassembly, and the programming of the robot was done through direct inputs from the user with either the teach pendant [14] or manual positioning [14]. This methodology has the advantage that it can be done by technicians without prior knowledge since the path planning is situationally dependent. The human brain is quickly able to make decisions as to how a system needs to be assembled or disassembled, and this process is not easily automated due to the highly complex nature of electro-mechanical systems. Research has been performed in the area of machine learning for the purpose of disassembly automation [14]. Oak Ridge National Laboratory has also started introducing an automated disassembly line to make battery recycling safer and faster [15]. Recently, some researchers reported studies on task planners for robot disassembly [16] and human-robot collaboration [17], but more research is required in this field.

In this study, a novel approach for disassembly of EV/HEV LIBs is presented based on the off-line simulation and path planning, as proposed to aid the implementation of the disassembly process. By using offline path planning, the precise control and tool paths of the robot can be predefined to maximize the efficiency of the required disassembly steps. In addition to this, both the robot dynamics and process time can be quantified to provide more insight into the state of the robot. By utilizing the CAD geometry models directly, offline simulation can be performed ahead of time, and allows the operator the ability to

precisely define waypoints within the model that can allow for alternative disassembly techniques.

## 2. Disassembly Workflow

To determine what steps in the disassembly process would be suitable for a robot, the manual disassembly process was observed and documented in Figure 1. The process of manual disassembly for the pack involved the following steps: (1) removal of the pack cover, (2) disconnection and removal of the main wiring harness and primary battery management system (BMS), (3) disconnection and removal of the thermal management system plumbing, (4) removal of the module tie downs, and (4) removal of the battery modules.

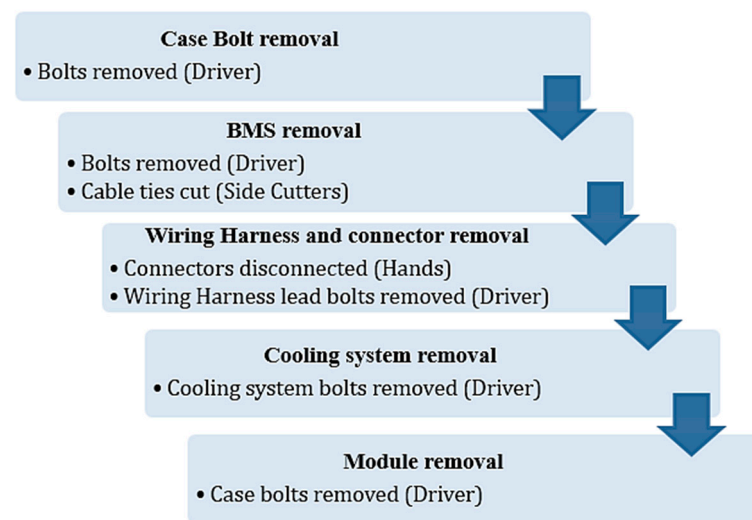


**Figure 1.** Disassembly process diagram of a battery pack by technician.

The disassembly of individual modules is comprised of the following: (1) the removal of the module BMS and main harness connector, (2) removal of the battery module frame bolts, (3) the removal of the module top cover, (4) the cutting of the first battery cell tabs, (5) the separation and removal of the first battery cell, and (6) the repetition of step 5 for the remaining cells. To describe the workflow of the disassembly process, one could maximize the use of the technician and robot by the following process, as depicted in Figure 2.

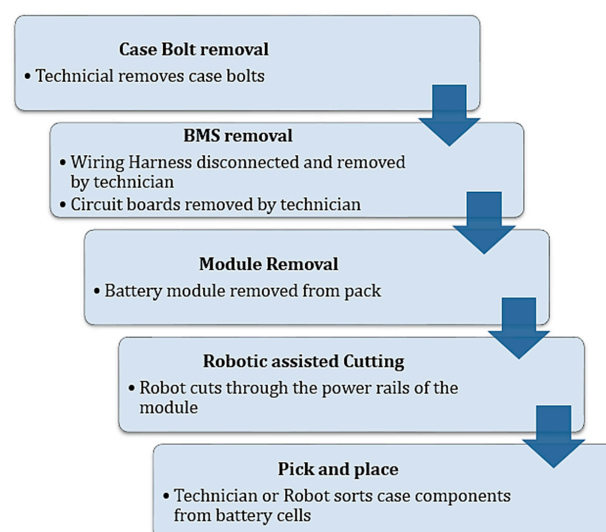


**Figure 2.** Process workflow as modified for a technician–robot collaboration.

### 3. Experimental Design for Human–Machine Collaboration

As the pack level disassembly of the case would require an industrial robot with a large reach as well as a high payload, it was decided that for the purposes of this experiment the scope of implementing a robot would be on the module disassembly level. A FANUC LR-Mate 200iD/4S, six degree of freedom (6DOF) industrial robotic system was used with a maximum payload of 4 kg and maximum reach of 550 mm. This robot was chosen due to its precision and small size, as well as having the ability to communicate with an end effector through the input/output port on the upper arm.

To prove the suitability of a robot for the disassembly of an EV/HEV battery system, the benchmark operations of cutting and gripping were selected for evaluation. Both the cutter and gripper are required for the disassembly process by the robot, and they are add-ins to the robot. Fine motor function, such as disconnection of electrical connectors, were decided to be outside the scope of this experiment, as the inherent level of complexity and dexterity needed would require more specialized end-of-arm tooling. A more generalized assessment of the robot's ability to perform gross motor function was chosen. The assessment was to be done for single end-effectors without accounting for the tool-change time, as a quick tool change and docking station could be implemented to automate the tool-change process. The total time for module disassembly would be evaluated based on the sum of the cutting and gripping operations, as well as any additional collaboration needed from a technician, such as fastener, connector, or harness removal. It is noted that the process analysis to find the total time of the disassembly process by robots is out of the scope of this paper.

End-of-arm tooling was a major focus of the experimental design, as the functional requirements defined in the robotic implementation stage required both highly precise motion and careful manipulation of components to prevent accidental shorting of the batteries or causing mechanical damage to the individual cells which could trigger a thermal event where explosion or fire could occur. Multiple modalities for the cutting tool were conceptualized, and a weighted decision matrix was used to select the best solution for implementation, design, and prototyping.

The first end effector to be evaluated was the cutting instrument, as this would be responsible for dismantling and separating the casing components from the individual battery cells. The cutting instrument would need to be compact, as the payload is limited to 4 kg, while maintaining the ability to cut through plastics and metal objects with both precision and speed. Cost was also considered a concern, as any additional cost of the robotic system would reduce the economic benefit. As listed in Table 1, the three modalities of cutting investigated were a high-speed rotary cutter, a reciprocating saw mechanism, and a laser-cutting instrument.

**Table 1.** Weighted decision matrix for three cutting methods.

Method	Cost (25)	Form Factor (5)	Heat Generation (15)	Vibration Amplitude (15)	Cut Precision (15)	Technical Implementation Difficulties (25)	Total (100)
Rotary cutter	25	5	10	10	13	25	88
Reciprocating cutter	20	4	15	5	5	15	64
Laser cutter	10	3	10	15	15	20	73

The high-speed rotary cutter was chosen due to the precision of cutting, compact size, and less technical difficulties, while still maintaining acceptable levels of heat generation and vibration transmission. Due to high-speed rotary cut-off tools being common, a Dremel 4000 was adapted to perform the cutting operations, as the motor and cutting speed were able to accommodate a wide range of materials and thicknesses. This was implemented, as shown in Figure 3a, and used in the offline simulation to represent the geometric properties.

Threads in the tool handle made cutting-tool integration with the robot secure and efficient. Since the state of the cutting tool only had one parameter that was controllable without modification of the tool, input/output states for the cutting tool can be controlled via a digital output as an on/off state from the upper arm in/out port communicating with a power relay to the tool.

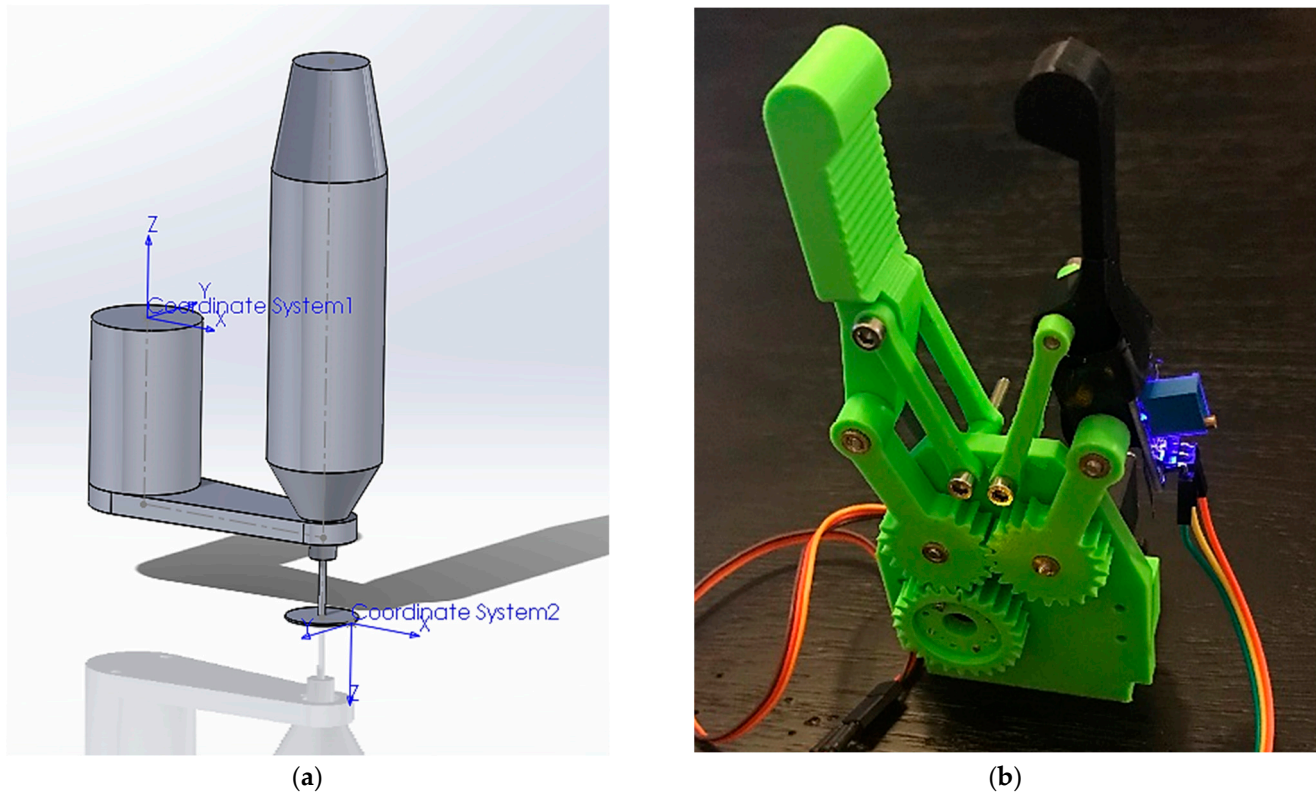


**Figure 3.** (a) The CAD model of the cutting tool, (b) the 3D-printed gripper with servo actuator and gear-driven coupled planar linkage system with force feedback.

After determining how to implement the cutting-tool control and designing custom mounting for it, the gripper was designed and built, as shown in Figure 3b. Most robotic cells have gripper attachments, but few control the exact gripping pressure or force that grippers use to interface components. This is particularly important in the case of LIBs, as mechanical damage to the battery cell can cause internal short circuit, leading to thermal runaway [18,19] which is a major hazard presented by LIBs. For the gripper to not damage battery cells, force regulation became an important feature in the gripper design. The primary design for the gripper was based on a servo-actuated, gear-driven coupled planar linkage system with force feedback as the feature to be controlled. This was done through the implementation of a strain gauge into the gripper's finger to measure the strain of the finger under load.

The finger was modeled as a fixed-free cantilever beam, where the load was applied at the tip of the finger. Knowing the geometric dimensions and the material properties of the as printed PLA, the Young's modulus, the beams cross sectional properties, and the length of the beam were used to determine the bending stress at the base of the beam through the bending-stress equation in Equation (1).

$$\sigma = \frac{My}{I} = \frac{FLh}{\frac{1}{6}bh^3}. \quad (1)$$

The force was then calculated from Equation (2) to determine how the input mapped to the output of the system for setting up the error value.

$$F = \frac{6L}{E\epsilon bh^2}. \quad (2)$$

The general design of the gripper was modeled as two gear-driven coupled four bar linkages with nearly parallel input links and four revolute joints to create a smooth motion. This allowed for a simplified actuation principle, as the system has only one degree of freedom being the input link angle if backlash and linkage compliance are assumed to be minimal. The general procedure was formulated similar to Ref. [20].

After determining how to observe the forces, a mathematical model for the system was created to implement a feedback control law for the system. This was derived through the use of Lagrange's equations. However, this yielded a sixth order nonlinear system of state equations for the planar linkage of the gripper. As a result of operating away from the nonlinear behavior, the system was approximated as a third order, linear, single input/single output (SISO) system, and the state space representation for the system dynamics was synthesized through the use of a least squares identification method. After synthesizing the state equations for use with the feedback error in the force, an infinite horizon linear quadratic regulator was implemented to control the system. For convenience and first try, the performance index, Q, and R matrices were selected as follows:

$$J = \int_{t_0}^{t_f} (x^T Q x + u^T R u) dt, \quad (3)$$

$$Q = \begin{bmatrix} 1 & 0 & 0 \\ 0 & 1 & 0 \\ 0 & 0 & 1 \end{bmatrix}, \quad R = [1].$$

The optimal gains were calculated through the solution to the algebraic Riccati equation (ARE) Equation (4) and implemented using state variable feedback, as shown below in Equations (5) and (6).

$$A^T S + SA + Q - SBR^{-1}B^T S = 0, \quad (4)$$

$$K = R^{-1}B^T S, \quad (5)$$

$$u = -Kx. \quad (6)$$

This was enough for the case of contacting the work piece. However, the initial conditions for solving the differential equations were not sufficient for the case of non-contact; thus, creating a two-step control strategy was required. As such, the gripper was modeled as a finite state machine with four states during operation. Due to the initial conditions not being available until after contact had been made with the work piece, four states were executed before the linear-quadratic regulator (LQR) control sequence was used. The first state was an idle state where the gripper was left in the state at which it last operated. After receiving an input signal from the robot during the pick and place sequence, the servo on the gripper moves the gripper to a limit open angle and sends a ready status to the robot in the form of a digital output. Once the robot moves the gripper into place for gripping the work piece, the robot then sends a start signal to the gripper to initiate a constant advance. After the contact force is detected via exceeding the contact force threshold, the initial conditions for the state equations are defined, and the LQR control sequence begins until the drop signal is given by the robot. The gripper controller was then tested for performance and implemented on the microcontroller through the Arduino toolbox in MATLAB, as shown in Figure 4.

Due to hazards associated with disassembly of a real battery system, a representative battery module was created that mimicked the geometry, layout, and material composition of the battery module observed in the manual disassembly. The construction of the module

consisted of a module frame, cell compartments that also functioned as cooling plates, top and bottom module covers, a front tab harness and connector, module frame bolts, and the module BMS. This was positioned on a flat surface within complete reach of the arm, where both cutting operations and pick and place could be completed. The representative module was made through the use of a 3D printer and assembled in a similar way to the actual module. The goal was to position the battery module in the workspace such that the tabs were accessible and that the individual cells could be lifted out from the top. Additionally, the module needed to remain in the same location during the cutting procedure; thus, the outline of the module location was marked, and the module was held in place with weights during the cutting operation.

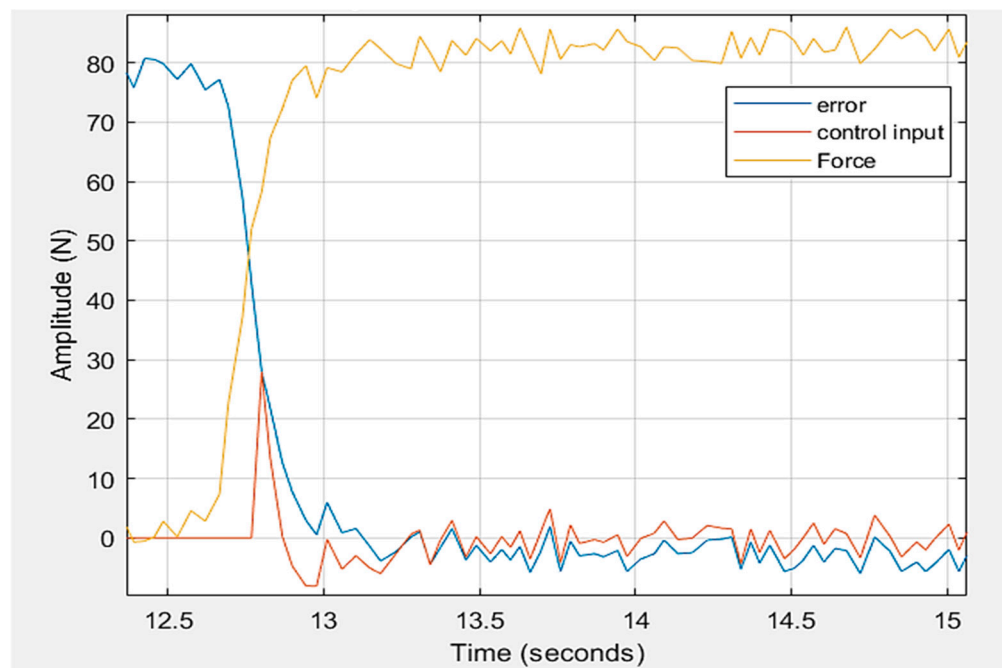


Figure 4. Gripper response under LQR control (results do not change if we increase the time).

To develop the kinematic model of the robot, the Denavit–Hartenberg (DH) representation of a kinematic linkage chain can be used to model the system in terms of the DH parameters,  $a_i, d_i, \theta_i, \alpha_i$ , as shown in Figure 5 [21].

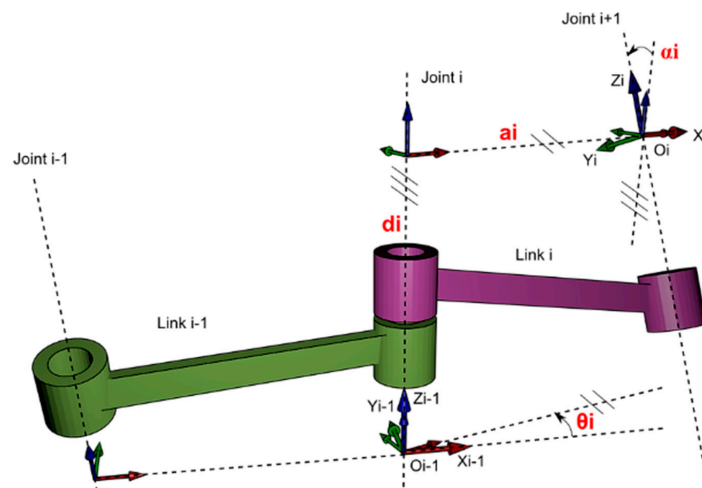


Figure 5. Parameter definitions of the Denavit–Hartenberg representation of a kinematic linkage chain.

For the case of the LR-Mate 200iD/4S, the DH parameters for the articulated robot are displayed in Table 2. J1-6 are the six links of the robot, and J7 is the end effector.

**Table 2.** DH parameters for the LR-Mate 200iD/4S [22].

Link	$\theta_i$	$d_i$	$a_i$	$\alpha_i$
J1	$\theta_1$	0	160	$\pi/2$
J2	$\theta_2$	0	330	0
J3	$\theta_3$	0	260	$\pi/2$
J4	$\theta_4$	290	0	$-\pi/2$
J5	$\theta_5$	0	0	$\pi/2$
J6	$\theta_6$	70	0	0
J7	0	107	100	$\pi/2$

Once the DH parameters are determined, the homogenous transformation matrix for each link can be computed as the product of the various rotation and translation matrices [21], as shown in Equation (7).

$${}^i T_i^{-1}(\alpha_i, \theta_i, a_i, d_i) = R_z(\theta_i) \times T_z(d_i) \times T_x(a_i) \times R_x(\alpha_i). \quad (7)$$

These equations are fundamental to both the forward and inverse kinematics solver for determining or solving the position and pose of the robot in space. Forward kinematics uses joint states to calculate a position given a specified pose of the robot, whereas inverse kinematics solve for the joint states of a given end effector position and pose. Solving the inverse kinematic equations is more difficult, as there can be multiple solutions or no solutions to a given end effector position.

Once the DH parameters are known along with all the masses and lengths of the links and end effector, one can use the following equation to solve for the torques required to move the robot joints to a desired location, and from there along a desired trajectory. This equation is often called the robot equation or the dynamic model for a robot.

$$\tau = D(q)\ddot{q} + h(q, \dot{q}) + C(q), \quad (8)$$

where  $\tau$  is the joint torques,  $D$  is the inertia matrix for all the links,  $h$  is Coriolis and centrifugal terms, and  $C$  is the gravity terms.

MathWorks' Robotics System Toolbox and Simscape Multibody Dynamics software packages were used in the MATLAB/Simulink environments to solve these equations. Both the forward and inverse kinematics/dynamics are simplified into blocks for use in solving the equations. There is a way to link CAD models directly into Simscape Multibody in the form of a Unified Robot Description Format (urdf) file. To import the robot model, the CAD model must be assembled, and the various coordinate systems, joint axes, inertia properties, and joint limits need to be defined during the setup of the urdf file. Once the urdf file is setup, it can be imported into MATLAB/Simulink, and motion analysis and offline path planning can be performed. Once the path planning was completed, simulation (Figure 6a) was performed in MATLAB/Simulink to evaluate the motion of various joint states. The waypoints as well as pose information (Figure 6b) were imported into MATLAB and fed into the inverse kinematics block in Simulink.

MATLAB utilizes the Levenberg–Marquardt algorithm (LMA) to solve the nonlinear least squares problem for the inverse kinematics. This method utilizes the minimization of the error in the joint configuration to that of the desired configuration to solve for the closest robot input joint angles to reach a target point [20,23]. This method is very robust and capable of solving complex motion tasks but can be slow to perform in real time. The Simulink block diagram for path definition and inverse kinematic is shown in Figure 7.

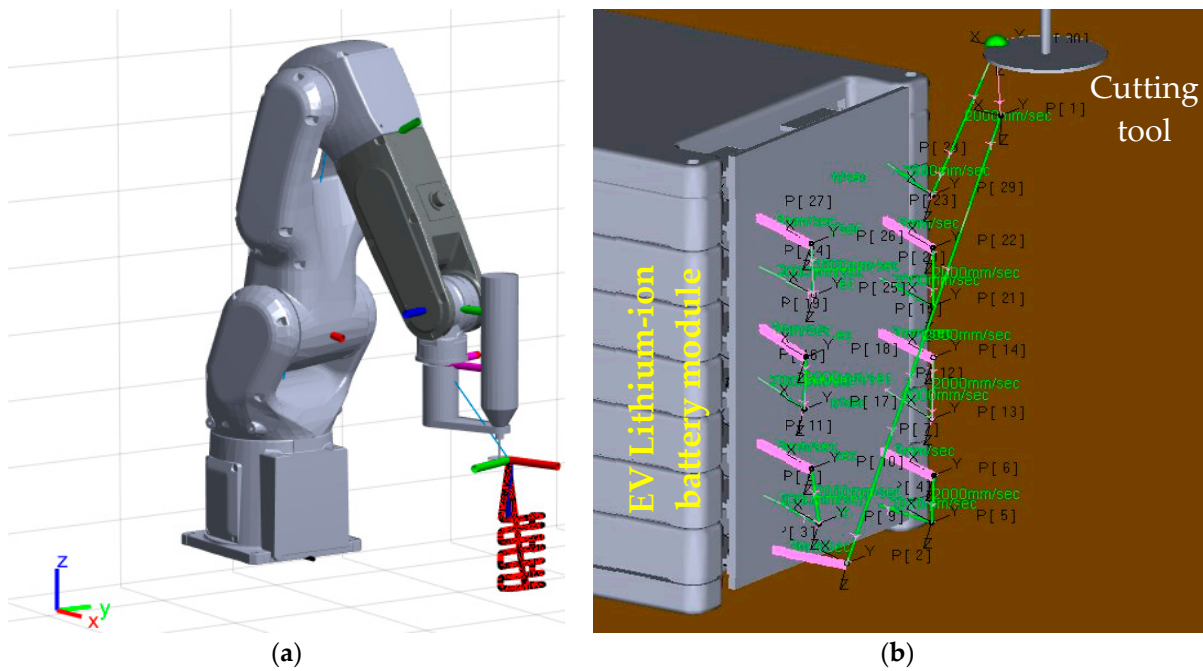


Figure 6. (a) Robot motion simulation to evaluate the motion of various joint states, (b) cutting path for a retired EV battery module to make it ready for recycling.

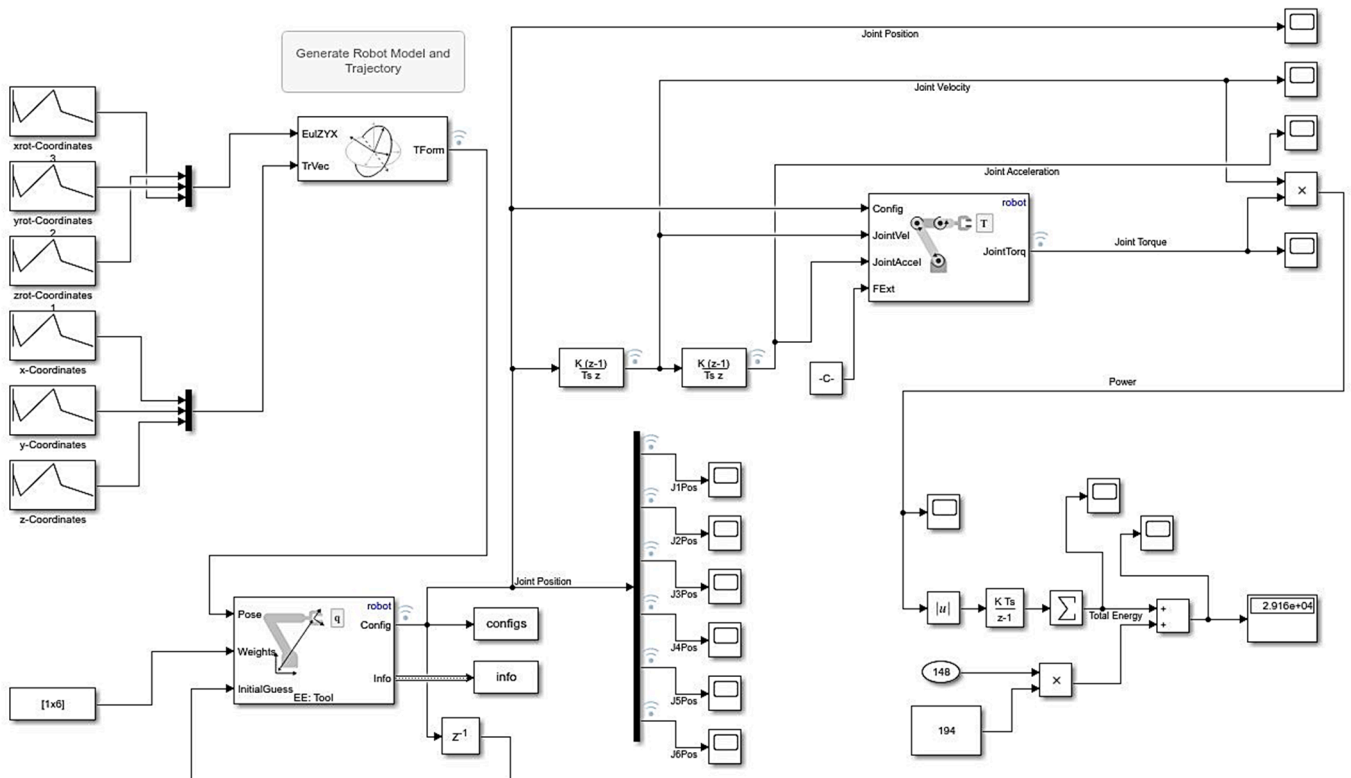


Figure 7. Simulink block diagram for path definition and inverse kinematic.

#### 4. Results and Discussion

The velocity, acceleration, and torque were obtained from the offline simulation of cutting an EV battery module and then plotted for each robot joint, as demonstrated in Figure 8, to study the involvement of each joint in the process. As seen in this figure, the

angular velocities for joint 2 and joint 5 were highest, and the angular acceleration for joint 5 and joint 7 were highest at the beginning and end of the process, as compared to other joints. The angular velocity and angular acceleration of all joints are fluctuating at the middle of the process; however, their values are not significantly greater than zero. The highest torque also belongs to joint 7, followed by joints 3 and 5. The torque of other joints remains close to zero during the process. As a remarkable result, it was revealed that all velocities, accelerations, and torques can be easily handled by the robot, as shown in the Figure 8. The error of values in Figure 8 depends on the accuracy of the model and the model input parameters. Our estimation is that the error of the Simulink simulation for the velocity, acceleration, and torque is less than 2%.

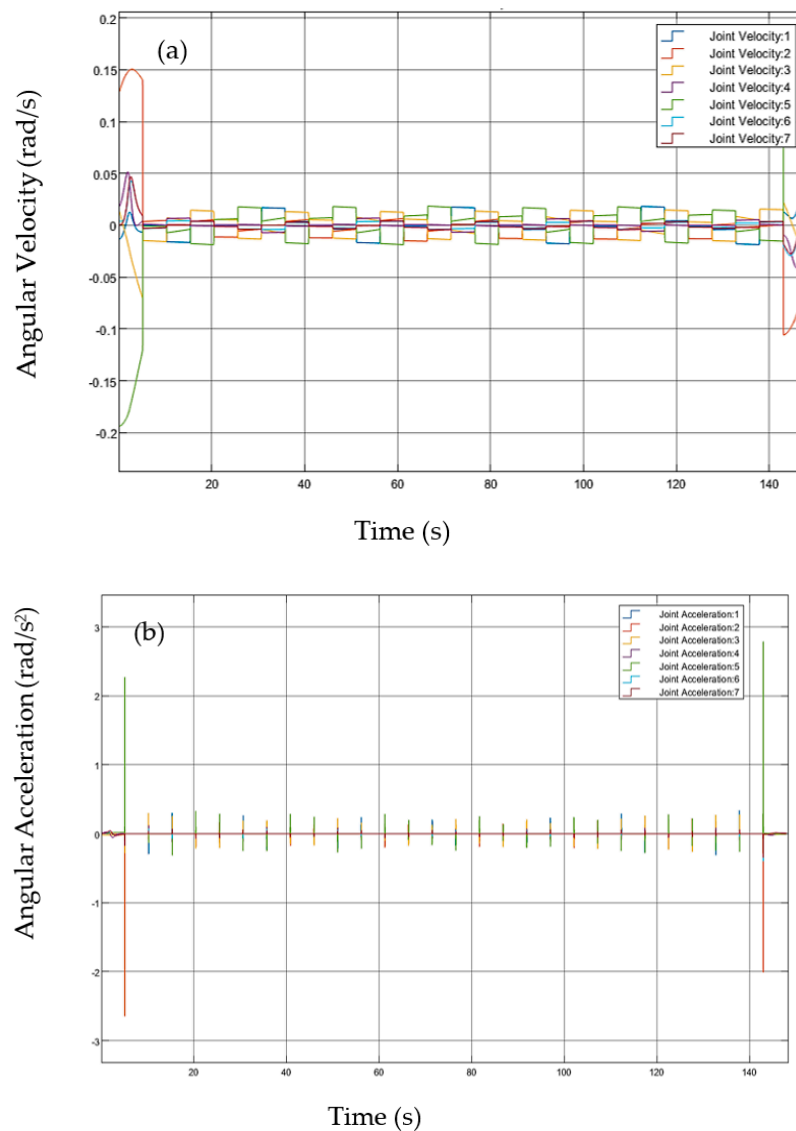
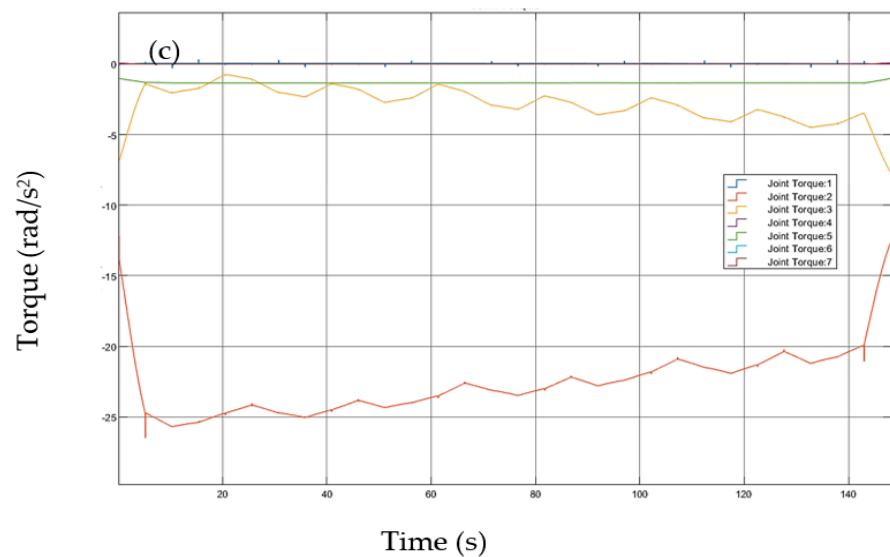


Figure 8. Cont.



**Figure 8.** The results of Simulink simulation: (a) joint angular velocity vs. time, (b) joint acceleration vs. time, (c) joint torque vs. time.

After the offline simulation was performed, the robot program was uploaded to the teach pendant to begin making the initial cuts experimentally. The cutting path was the first item to be tested in the experiment. The quality of the cut was based on two performance metrics:

1. accuracy of the cut and
2. disruption of the work piece within the workspace.

All battery tabs in the EV battery modules (the LIB cells are the pouch type) were successfully cut by the robot (See Figure 9). The cutting tool placed the cut with both accuracy and speed, performing the operation in 112 s (1:52 min). A technician completed this operation in 220 s (3:40 min) in the LIB recycling plant, which is 108 s (1:48 min) longer than the robot. This almost a 2X gain in speed efficiency. Thus, the disassembly process may be two times faster when a robot is incorporated into the process. However, more detailed time analysis is required for the final answer.

However, more importantly, the cutting path developed for the robot was more efficient, as it was a continuous cutting process and did not require the tool to be changed. Pick-and-place operations proved to be slightly lengthier and less successful in both time and performance compared to the technician. Therefore, the best option for disassembly of a LIB pack/module would be a human and robot collaboration, where the robot could make efficient cuts on the battery pack, and the technician/laborer could quickly sort the battery components and remove connectors or fasteners with which the robot would struggle. This is based on the results of the experiment, as the technician is capable of sorting through the components of the battery module 18 s faster than the robot and with higher rates of success.

The readers are referred to Ref. [24], the publication of the authors at ASME IMECE-2019 for more information on the design aspect of this project. For more information about recycling lithium-ion batteries, the readers are recommended to look at Refs. [25–27].

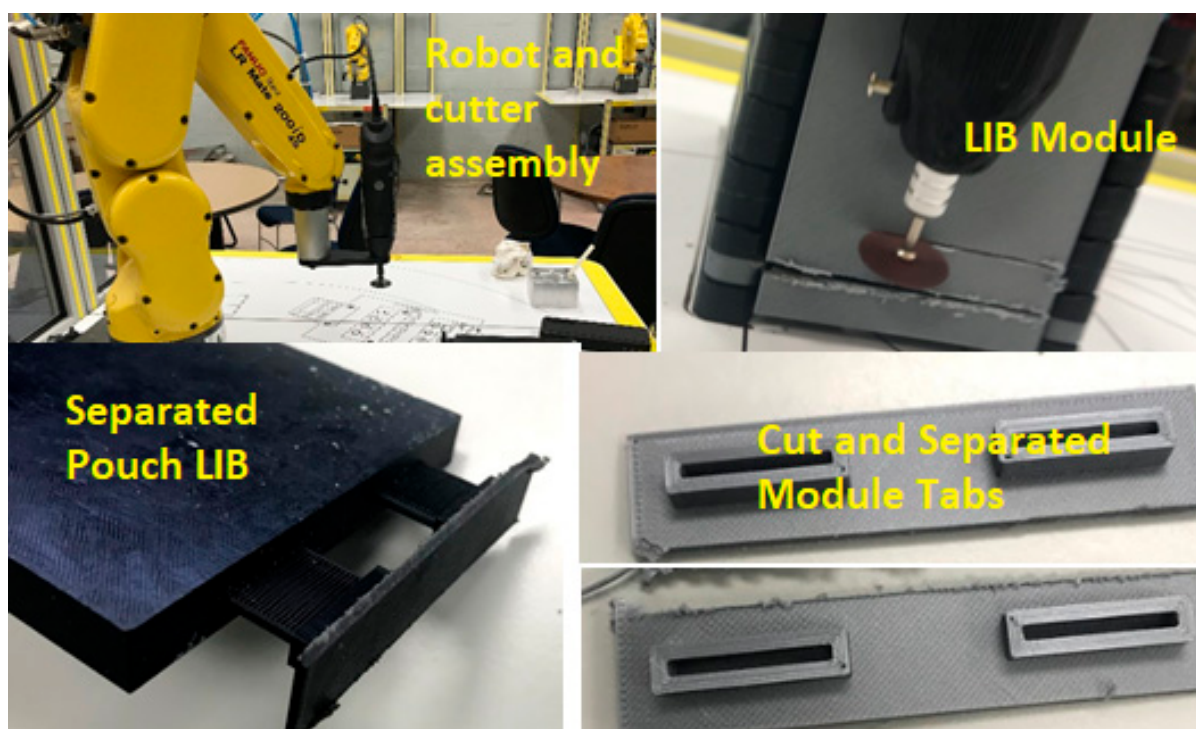


Figure 9. The results of the implementation of the work experimentally.

## 5. Conclusions

In this study, a method for the robotic disassembly of an electric vehicle battery module was proposed and tested. Offline simulation was used to perform path planning for the disassembly of the battery module, and custom end-of-arm tooling was designed. The cutting tool demonstrated improvements in effectiveness over a purely technician-based disassembly due to the precision of the cuts made by the robotic arm. The cutting speed and direction did have a significant influence on the cut quality, as too high of a speed would increase the temperature, and too low of a speed would stall the motor. In the experimental testing of the cutter, the robotic arm was extremely capable in making the required cuts, and the only instances it failed were when the mock battery module was not properly secured to the workspace. A way of controlling the gripper to utilize force regulation was designed using system identification techniques in the form of a batch least squares estimator. This was then utilized to form a state space representation for the gripper, and a linear quadratic regulator was implemented to determine the optimal gains required to control the system. Despite the development of a customized gripper under LQR control, the pick-and-place operations proved to be more of a challenge, as the control sequence was slow to sense contact with the part, and the geometry of the gripping tool was not able to securely hold on to the battery cell. This could be overcome through redesigning the gripper fingers, choosing more rigid construction materials, and developing a faster sensing method for contact detection. As a remarkable result, it can be concluded that the best option for disassembly of a LIB pack would be human and robot collaboration, where the robot could make efficient cuts on the battery pack, and the technician could quickly sort the battery components and remove connectors or fasteners with which the robot would struggle. This collaboration also reduces the danger encountered by the technician because the risk of shorting battery cells while cutting would be eliminated, and sharing in the labor contribution reduces the required man hours for disassembling an EV battery module or pack. The focus of this study was the technical aspects of the disassembly of EV/HEV LIBs by industry robots. The continuation of this work can be an economic analysis and studying the time saving in the disassembly process when the human–robot collaboration approach is chosen.

**Author Contributions:** Data curation, I.K.; Formal analysis, I.K., S.F., A.M., R.E. and S.R.H.; Funding acquisition, S.F.; Investigation, I.K. and S.F.; Methodology, I.K. and S.F.; Resources, S.F.; Software, S.F.; Supervision, S.F. and A.M.; Validation, I.K.; Writing—original draft, I.K., R.E. and S.R.H.; Writing—review & editing, S.F. and A.M. All authors have read and agreed to the published version of the manuscript.

**Funding:** This research received no external funding.

**Acknowledgments:** This work would not have been possible without the help of Don Goode and Ed Green from Retriev Technologies, the University of Akron for providing the necessary software and hardware resources and financial support, Ohio Department of Higher Education, and the RAPIDS program for funding the robot cells. A part of this paper has been presented at the ASME IMECE conference in 2019, Paper No: IMECE2019-11949, entitled “Robotic Disassembly of Electric Vehicle Battery Systems” by the authors.

**Conflicts of Interest:** The authors declare no conflict of interest.

## Nomenclature

A	A matrix
b	width of cantilever beam (mm)
F	applied force (N)
B	B matrix
E	Young’s modulus (GPa)
h	thickness of cantilever beam (mm)
I	second moment of area (mm <sup>4</sup> )
M	bending moment (N.m)
l	length of beam (mm)
$\epsilon$	strain
$a_i$	length of common normal (m)
$d_i$	offset along z-axis to common normal (m)
$\theta_i$	angle about previous z (degrees)
$\alpha_i$	angle about common normal (degrees)
J	performance index
x	generalized coordinate (mm/degrees)
Q	weighting matrix on the position
R	weighting matrix on the control input
u	control input
K	optimal gain
S	variable used for the ARE
T	homogenous transformation matrix
$R_z(\theta_i)$	rotation matrix about z axis
$T_z(d_i)$	translation matrix along z
$R_x(\alpha_i)$	rotation matrix about x
$T_x(a_i)$	translation matrix along x

## Abbreviation

BMS	battery management system
EOL	end of life
HEV	hybrid electric vehicles
IC	integrated circuits
LQR	linear quadratic regulator
LIB	lithium-ion battery
PCB	printed circuit board

## References

1. Wang, L.; Wang, X.; Yang, W. Optimal design of electric vehicle battery recycling network—From the perspective of electric vehicle manufacturers. *Appl. Energy* **2020**, *275*, 115328. [[CrossRef](#)]

2. Zhang, L.; Li, L.; Rui, H.; Shi, D.; Peng, X.; Ji, L.; Song, X. Lithium recovery from effluent of spent lithium battery recycling process using solvent extraction. *J. Hazard. Mater.* **2020**, *398*, 122840. [[CrossRef](#)] [[PubMed](#)]
3. Thompson, D.L.; Hartley, J.M.; Lambert, S.M.; Shiref, M.; Harper, G.D.; Kendrick, E.; Anderson, P.; Ryder, K.S.; Gaines, L.; Abbott, A.P. The importance of design in lithium ion battery recycling—a critical review. *Green Chem.* **2020**, *22*, 7585–7603. [[CrossRef](#)]
4. Mohr, M.; Peters, J.F.; Baumann, M.; Weil, M. Toward a cell-chemistry specific life cycle assessment of lithium-ion battery recycling processes. *J. Ind. Ecol.* **2020**, *24*, 1310–1322. [[CrossRef](#)]
5. Bai, Y.; Muralidharan, N.; Sun, Y.-K.; Passerini, S.; Whittingham, M.S.; Belharouak, I. Energy and environmental aspects in recycling lithium-ion batteries: Concept of Battery Identity Global Passport. *Mater. Today* **2020**, *41*, 304–315. [[CrossRef](#)]
6. Sloop, S.; Crandon, L.; Allen, M.; Koetje, K.; Reed, L.; Gaines, L.; Sirisaksoontorn, W.; Lerner, M. A direct recycling case study from a lithium-ion battery recall. *Sustain. Mater. Technol.* **2020**, *25*, e00152. [[CrossRef](#)]
7. Buss, S.R. Introduction to inverse kinematics with jacobian transpose, pseudoinverse and damped least squares methods. *IEEE J. Robot. Autom.* **2004**, *17*, 16.
8. Dang, H.; Wang, B.; Chang, Z.; Wu, X.; Feng, J.; Zhou, H.; Li, W.; Sun, C. Recycled Lithium from Simulated Pyrometallurgical Slag by Chlorination Roasting. *ACS Sustain. Chem. Eng.* **2018**, *6*, 13160–13167. [[CrossRef](#)]
9. Vieceli, N.; Nogueira, C.A.; Guimarães, C.; Pereira, M.F.C.; Durão, F.O.; Margarido, F. Hydrometallurgical recycling of lithium-ion batteries by reductive leaching with sodium metabisulphite. *Waste Manag.* **2018**, *71*, 350–361. [[CrossRef](#)]
10. Wang, H.; Friedrich, B. Development of a Highly Efficient Hydrometallurgical Recycling Process for Automotive Li-Ion Batteries. *J. Sustain. Metall.* **2015**, *1*, 168–178. [[CrossRef](#)]
11. Gaines, L. The future of automotive lithium-ion battery recycling: Charting a sustainable course. *Sustain. Mater. Technol.* **2014**, *1–2*, 2–7. [[CrossRef](#)]
12. Tanong, K.; Blais, J.-F.; Mercier, G. Metal recycling technologies for battery waste. *Recent Pat. Eng.* **2014**, *8*, 13–23. [[CrossRef](#)]
13. Heelan, J.; Gratz, E.; Zheng, Z.; Wang, Q.; Chen, M.; Apelian, D.; Wang, Y. Current and prospective Li-ion battery recycling and recovery processes. *Jom* **2016**, *68*, 2632–2638. [[CrossRef](#)]
14. Wegener, K.; Chen, W.H.; Dietrich, F.; Dröder, K.; Kara, S. Robot Assisted Disassembly for the Recycling of Electric Vehicle Batteries. *Procedia CIRP* **2015**, *29*, 716–721. [[CrossRef](#)]
15. Available online: <https://www.ornl.gov/news/automated-disassembly-line-aims-make-battery-recycling-safer-faster> (accessed on 23 June 2022).
16. Choux, M.; Marti Bigorra, E.; Tyapin, I. Task Planner for Robotic Disassembly of Electric Vehicle Battery Pack. *Metals* **2021**, *11*, 387. [[CrossRef](#)]
17. Gerbers, R.; Wegener, K.; Dietrich, F.; Dröder, K. Safe, Flexible and Productive Human-Robot-Collaboration for Disassembly of Lithium-Ion Batteries. In *Recycling of Lithium-Ion Batteries. Sustainable Production, Life Cycle Engineering and Management*; Kwade, A., Diekmann, J., Eds.; Springer: Berlin/Heidelberg, Germany, 2018. [[CrossRef](#)]
18. Doughty, D.H.; Roth, E.P. A general discussion of Li ion battery safety. *Electrochem. Soc. Interface* **2012**, *21*, 37–44.
19. Kong, L.; Li, C.; Jiang, J.; Pecht, M.G. Li-ion battery fire hazards and safety strategies. *Energies* **2018**, *11*, 2191. [[CrossRef](#)]
20. Nakamura, Y.; Hanafusa, H. Inverse kinematic solutions with singularity robustness for robot manipulator control. *J. Dyn. Sys. Meas. Control.* **1986**, *108*, 163–171. [[CrossRef](#)]
21. Spong, M.W.; Hutchinson, S.; Vidyasagar, M. *Robot Modeling and Control*; Wiley: Hoboken, NJ, USA, 2006.
22. FANUC. *FANUC Robot LR-Mate 200iD*; FANUC America Corporation: Rochester Hills, MI, USA, 2013; pp. 48309–48325. Available online: [https://www.fanucamerica.com/docs/default-source/robotics-product-information-sheets/lr-mate-200id-series\\_187.pdf?sfvrsn=acc1fb06\\_4](https://www.fanucamerica.com/docs/default-source/robotics-product-information-sheets/lr-mate-200id-series_187.pdf?sfvrsn=acc1fb06_4) (accessed on 10 April 2019).
23. Wampler, C.W. Manipulator inverse kinematic solutions based on vector formulations and damped least-squares methods. *IEEE Trans. Syst. Man Cybern.* **1986**, *16*, 93–101. [[CrossRef](#)]
24. Kay, I.; Esmaeeli, R.; Hashemi, S.R.; Mahajan, A.; Farhad, S. Recycling Li-ion Batteries: Robot Disassembly of Electric Vehicle Battery Systems, IMECE2019-11949. In Proceedings of the ASME 2019, International Mechanical Engineering Congress and Exposition (IMECE), Salt Lake City, UT, USA, 11–14 November 2019.
25. Al-Shammari, H.; Farhad, S. Performance of Cathodes Fabricated from Mixture of Active Materials Obtained from Recycled Lithium-Ion Batteries. *Energies* **2022**, *15*, 410. [[CrossRef](#)]
26. Al-Shammari, H.; Farhad, S. Heavy Liquids for Rapid Separation of Cathode and Anode Active Materials from Recycled Lithium-Ion Batteries. *Resour. Conserv. Recycl.* **2021**, *174*, 105749. [[CrossRef](#)]
27. Farhad, S.; Gupta, R.K.; Yasin, G.; Nguyen, T.A. *Nanotechnology for Battery Recycling, Remanufacturing, and Reusing*; Elsevier: Amsterdam, The Netherlands, 2022; ISBN 13978-0323911344.